ELSEVIER

Journal of Power Sources 99 (2001) 15–25

JOURNAL OF POWER SOURCES

www.elsevier.com/locate/jpowsour

# On the misuse of the crystal structure model of the Ni electrode material

Ulrik Palmqvist[a], Lars Eriksson[b,*], Javier García-García[a], Nina Simic[c], Elisabet Ahlberg[c], Rune Sjövall[d]

[a]*Inorganic Chemistry, Arrhenius Laboratory, Stockholm University, SE-106 91 Stockholm, Sweden*
[b]*Structural Chemistry, Arrhenius Laboratory, Stockholm University, SE-106 91 Stockholm, Sweden*
[c]*Department of Chemistry, Göteborg University, SE-412 96 Göteborg, Sweden*
[d]*Saft AB, Jungnergatan, P.O. Box 709, SE-572 28 Oskarshamn, Sweden*

Received 3 July 2000; received in revised form 7 November 2000; accepted 20 November 2000

**Abstract**

Ni–Cd pocket plate single cells have been float-charged at 1.40 and 1.42 V at room temperature and 40°C for a time period of 2–3 years. Subsequent ex situ X-ray diffraction measurements were performed on the charged positive active Ni electrode material.

The appearance of the diffraction pattern of one of the charged electrode materials (conventionally named nickel oxy-hydroxide-β-NiOOH) shows resemblance to the pattern of discharged nickel hydroxide (β-$Ni(OH)_2$). In situ X-ray diffraction, electrochemical and transmission electron microscopy measurements were used to further investigate this charged phase.

Our results clearly show the difficulties to interpret the data from X-ray powder diffraction measurements in order to study and characterise aged positive active material, especially in the charged state. The use of structure models from well crystalline, often synthetically manufactured, powder samples in order to describe amorphous material must be questioned. There are numerous parameters that may affect the charge/discharge transformation and the structural appearance of positive active material.

Transmission electron microscopy (TEM) measurements indicate structural differences of the sample subjected to Rietveld refinement on X-ray diffraction data compared to earlier published structure. 

*Keywords:* β-$Ni(OH)_2$; β-NiOOH; Ni electrode; Float charging; XRD; TEM

## 1. Introduction

The alkaline Ni–Cd battery is a mature product [1]. Over the years, various designs have been developed from pocket-plate, tubular and sintered cells to more sophisticated foam and plastic bonded electrode cells. Common for these designs are the use of nickel hydroxide and cadmium hydroxide as active materials, which during charging transform to nickel oxy-hydroxide and free cadmium. Nickel hydroxide and its oxidation products are of special interest, since it constitutes the positive electrode in other battery systems, e.g. Ni–MeH, Ni–Zn and Ni–$H_2$.

The redox process of the positive active material induces several different structural changes. Its behaviour is depending on for example temperature, electrolyte concentration, extent of discharge/charge and iron content. In efforts made to understand the Ni electrode material, it has been extensively examined by X-ray diffraction (XRD), extended X-ray absorption fine structure (EXAFS), Raman spectroscopy, neutron diffraction and infra-red spectroscopy (IR). A large number of scientific papers have been generated in the fields of electrochemistry, structural chemistry and applied battery technology.

From a structural point of view, the nickel hydroxide and oxy-hydroxide phase transformations have been of particular interest. However, problems arise on determination of the structure of these phases by XRD due to the highly disordered or amorphous nature of the material. The transformations are believed to be largely heterogeneous [2], and the discharge mechanism (Ni(III) to Ni(II)) is thought to progress through either of two types of reactions (a) proton diffusion mechanism or (b) by an intercalated water mechanism [3]. It is difficult to separate the oxidised and reduced phases, since they have been suggested to have closely related structures [4]. McEwen [5] claims that the oxidation rate determines to what extent the discharged β-$Ni(OH)_2$ structure is preserved in the charged β-NiOOH

* Corresponding author. Tel.: +46-08-16-2394; fax: +46-08-16-3118.
*E-mail address*: lerik@struc.su.se (L. Eriksson).

0378-7753/01/$ – see front matter 
PII: S0378-7753(00)00676-5

state. Barnard et al. [6] state that the differences between the charged and discharged structures only originate from differences in intensities of the XRD peaks. The oxidation of β-$Ni(OH)_2$ occurs topotactically and the decreasing line intensities are followed by a defect layer structure. Briggs and Wynne-Jones [4] claim that the discharged structure persists almost unchanged upon oxidation to a composition of about $NiO_{1.35}$, whereas Feitknecht et al. [7] believe that under some circumstances the divalent Ni structure can persist up to trivalent Ni ($NiO_{1.5}$).

A reaction scheme for the transformation between the different phases was initially proposed by Bode et al. in 1966 [8]. Their scheme is still valid, although some changes have been proposed. The existing phases can be summarised as follows. β-$Ni(OH)_2$, the discharged state, exhibits hexagonal close packing (hcp) of oxygen. The space group is *P31m* (1 6 2) and the lattice parameters are $a = 3.126$ Å, $c = 4.605$ Å (JCPDS 14-0117) [9]. The structure is described as a layered structure along the *c*-axis with a hexagonal arrangement of nickel in each layer and oxygen octahedrally coordinated, similar to the brucite structure ($Mg(OH)_2$) (cf. Fig. 1). Evidenced by IR, Oliva et al. [10] state that there are no hydrogen bonds between the layers.

β-NiOOH, the charged state, has the valence 3+, which has been proved by X-ray absorption near-edge structure (XANES) measurements [11]. This phase is suggested to exhibit a hexagonal lattice, similar to that of β-$Ni(OH)_2$. The lattice parameters are $a = 2.81$ Å, $c = 4.84$ Å (JCPDS 06-0141) [9]. The protons are intercalating between the layers, building up a hydrogen-bonded structure, indicated by IR [10]. Malsbury and Greaves [12] show that $Ni_2O_3H$ exhibits a largely different diffraction pattern compared to the β-NiOOH, and presents an orthorhombic unit cell, however, with a close relation to the unit cell of β-NiOOH, where the valence of nickel is alternating between 4+ and 2+. There are still questions about the structural appearance of β-NiOOH not answered by the conventional hexagonal ($a = 2.8$ Å and $c = 4.8$ Å) structure model.

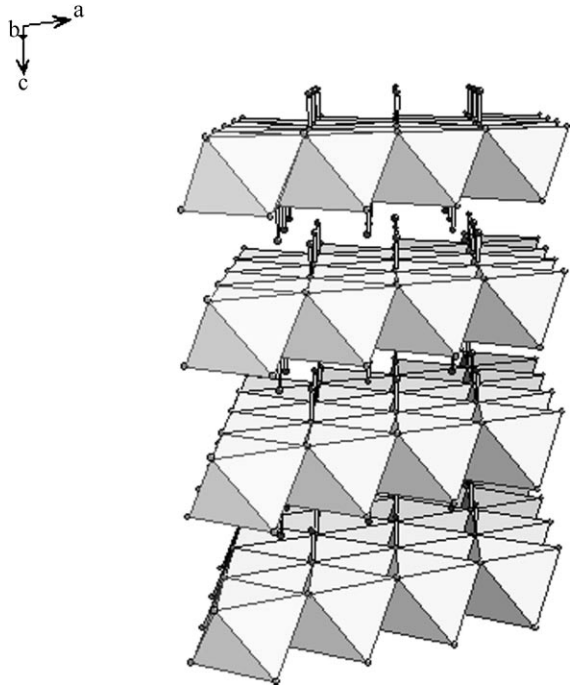


Fig. 1. Structure of hexagonal β-$Ni(OH)_2$, showing the layered structure along the (0 0 1) direction. The Ni atoms are located at the centre of the octahedron and O at the vertices. H is pointing outwards perpendicular to each layer.

Overcharging of the β-$Ni(OH)_2$ may give γ-NiOOH phase. This phase has a 2.82 Å Ni–Ni distance, but the interlayer distance is thought to vary in a wide range due to intercalation of alkali cations (e.g. $Li^+$, $K^+$), water molecules, and due to the stacking sequence of the $NiO_2$ layers. A typical value of the interlayer distance is around 7 Å. Discharging occurs via an intermediate phase, α-$Ni(OH)_2$, to β-$Ni(OH)_2$, or directly from γ-NiOOH to β-$Ni(OH)_2$ [13].

The aim of the present work is to contribute to the existing knowledge concerning the structural description of the active nickel material and to discuss the present model in a critical view. Throughout the course of this work, ordinary pocket plate single cells have been used. These cells have been float-charged at room temperature (RT) and at 40°C for more than 2 years, float-charged at 1.40 and 1.42 V constant voltage, respectively. The structural appearance of one of the charged positive active materials (float-charged at room temperature and 1.42 V) could not easily be explained on examination by X-ray powder diffraction and was, therefore, further investigated by in situ XRD and transmission electron microscopy (TEM) measurements.

The conclusions from our experiments are that the use of crystal structure models from well-crystalline powder samples, often synthetically manufactured, and from possibly single crystal experiments to describe heavily disordered, even amorphous and aged Ni electrode materials can be greatly questioned.

The TEM measurements indicate a much longer *c*-axis, independently determined from several different crystallites, on one of the positive discharged electrode materials. The *c*-axis was determined to be $c = 5.0(1)$ Å from all crystallites. Furthermore, systematic extinctions were found in the (0 0 *l*) reflections that indicated the presence of translational symmetry elements not present in the conventional structure model of β-$Ni(OH)_2$.

## 2. Experimental

### 2.1. Test cells

Three types of pocket plate single cells, denoted [A], [B] and [C] in the following, were tested electrically. The positive electrode consists mainly of nickel hydroxide and graphite, and the negative electrode of cadmium hydroxide, iron oxide and graphite. The aged electrolyte consists of an aqueous solution of KOH, LiOH and $K_2CO_3$ [14].

### 2.2. Electrical testing

Prior to the electrical testing, the cells were subjected to two formation cycles at RT in order to activate the electrode material. The formation was followed by capacity measurements at $0.2C_5$ A. Then the cells were either charged at a constant potential of 1.42 V at RT during 2 years [A], at a constant potential of 1.40 V and 40°C during 3 years [B], or at constant potential of 1.42 V at 40°C during 3 years [C]. Cell and electrode capacity measurements were conducted directly after these charging periods. The capacity data were registered by means of a computer-controlled sampling system.

### 2.3. Cell dismantling

After the electrical testing, the cells used for analyses were further cycled in order to eliminate γ-NiOOH. The cycle route was concluded with charging 10 h at $0.2C_5$ A in order to assure the state of charge of the positive electrode.

Then the positive electrodes were dismantled in the charged state. The active material was immediately transformed into a vacuum vessel and dried at low pressure for 2 h to achieve a gentle and fast drying. The drying process was either performed at RT or at 60°C. After the drying, the sample was immediately analysed with X-ray diffraction and electrochemical techniques.

### 2.4. Ex situ XRD measurements

The samples were examined by X-ray diffraction using a powder diffractometer SIEMENS D5000. During the powder analysis, the diffractometer was equipped with either a position sensitive detector (PSD) or a scintillation detector. A copper characteristic radiation source was used ($\lambda = 1.54184$ Å). The measurements were made at 0.02° intervals of $2\theta$ using a cumulated count-time of 10 s for each step over the range 10–70° in $2\theta$ when the PSD was used, and 10–90° when the scintillation detector was used.

Rietveld refinements were performed on intensity data from the charged Ni electrode material [A] with silicon added as an internal standard.

Crystallite sizes from the (0 0 1), (1 0 0) and (1 0 1) peaks of the various nickel hydroxide/oxy-hydroxide phases were calculated by the Scherrer formula, with a value of 0.9 for the Scherrer constant $K$ [15].

$$L = \frac{K\lambda}{\beta \cos\theta}$$

where $L$ is the mean dimension of the crystallites (Å) and $\beta$ the breadth of the diffraction peak (radians) corrected for instrumental effects. For these calculations, the Philips PC-APD program version 4.0e was used. Corrections for instrumental effects on peak broadening were made by using the full widths at half height of properly-chosen silicon lines.

### 2.5. In situ XRD measurements

In situ XRD measurements were performed on the active material [A] and with a set-up described below and shown in Fig. 2.

To collect X-ray powder diffraction patterns, a STOE Stadi-P diffractometer was used equipped with a Ge monochromator and a linear PSD covering 6° in $2\theta$.

The experimental construction consists of a Teflon® (PTFE) cell covered with a polyethylene (pe) window fixed with a stainless steel ring. This window material is mechanically robust and chemically inert, and at the same time sufficiently transparent to X-rays. Polyethylene exhibits quite a low absorption coefficient $\mu = 8.876\ \text{cm}^{-1}$ [16]. The positive and negative electrodes were manufactured as described below. A 0.60 g of the material [A] (≈100 mAh) and 0.60 g of negative active $Cd(OH)_2$ material (≈190 mAh) was used. The electrolyte was 6 M KOH aqueous solution. Circular sheets of 18 and 25 mm in diameter were cut from a nickel mesh. The 25 mm disc was fringed and a small hole ($\varnothing \approx 2$ mm) was cut out in the middle of the disc. A circular tablet of 18 mm of the active material was compacted at a pressure of 20 MPa and placed on the larger fringed disc upon which the smaller disc and a tab was placed. The fringes were folded back and the whole package was compacted at a pressure of 10 MPa. A Ni plate was used as reference electrode. In order to prevent short-circuits and at the same time assure that the electrodes still achieve good wettability, they were separated by polypropylene (pp) fibrous separators.

Prior to the in situ X-ray measurements, the cell was cycled several times at $0.2C_5$ A, and finally charged with $0.1C_5$ A. The X-ray diffraction measurements were thereafter performed during 24 h at constant charging rate of $0.05C_5$ A. The subsequent discharge was monitored in order to qualitatively be able to deduce the chargeability of the Ni electrode. X-ray measurements were performed on discharged materials as well.

### 2.6. Electrochemical investigation

In order to investigate the state of charge of material [A] studied by ex situ XRD, electrochemical techniques were employed. A conventional three-electrode cell was used with platinum gauze as the auxiliary electrode. The potential at the working electrode was measured against a saturated potassium chloride reference Ag/AgCl electrode, $E = 220$ mV with respect to SHE. The working electrode was made of the positive active material mixed with a carbon paste, using the carbon paste electroactive electrode (CPEE) technique. This technique, which can be used to study the electrochemical behaviour of powders and non-conducting materials, has been described elsewhere [14,17,18]. The mixing ratios (by weight) were 1:3 E/CP (electroactive material/carbon paste). The cell was made of polypropylene and all experiments were carried out at room temperature. The electrolyte used consisted of 3.5 M KOH, 0.75 M LiOH

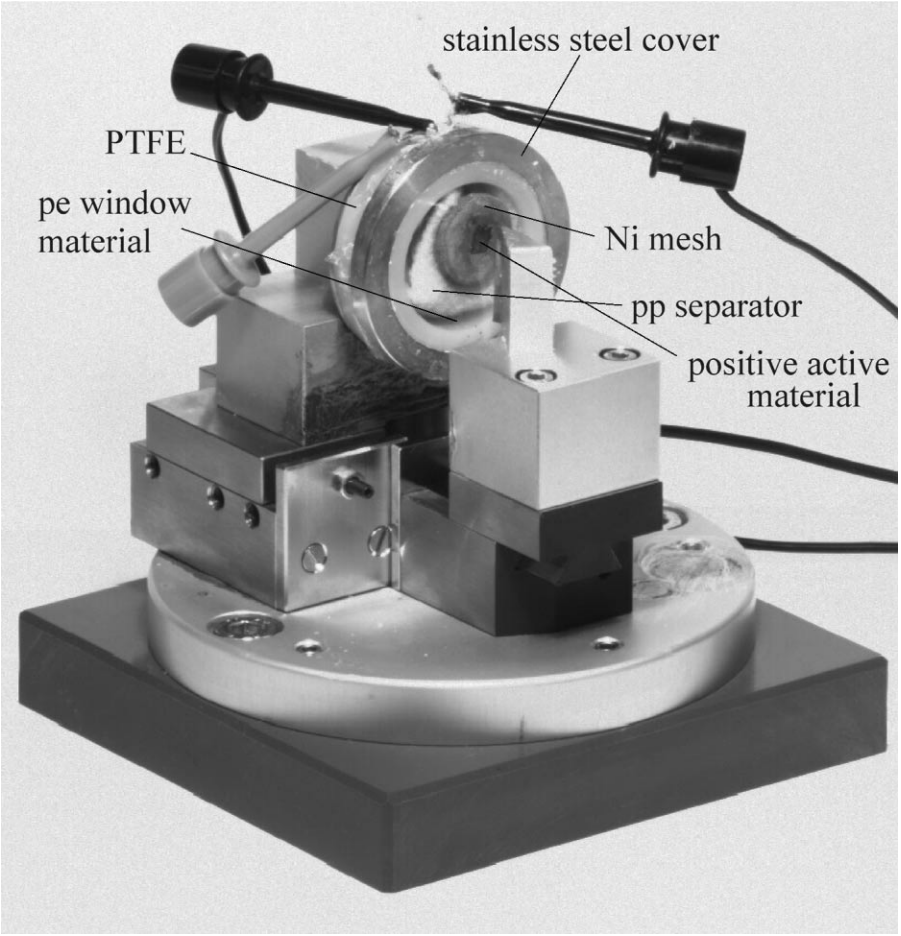


Fig. 2. The appearance of the cell used in the in situ XRD measurements.

and 0.75 M $K_2CO_3$ in order to simulate the electrolyte composition found in the batteries. In order to prevent oxygen contamination, the electrolyte was purged with highly-purified nitrogen for at least 30 min before the experiment, and a nitrogen flow was maintained above the solution during the measurements as well in order to keep the inert atmosphere. An EG&G Princeton Applied Research Potentiostat/Galvanostat Model 273A was used equipped with the 270 software package.

The state of charge of the active material was determined by electrochemical reduction of the active material to metallic nickel. The reduction was performed by chronopotentiometry and by potential sweep techniques. A constant current of −0.1 mA was applied, with a time length depending on the amount of active material at the carbon paste electrode surface. The potential sweep rate used was 0.1 mV/s.

### 2.7. TEM measurements

TEM was performed on discharged material [A], which was washed in water and dried at 70°C overnight before use. The samples were prepared by grinding in ethanol and placing one drop of the suspension onto a holey carbon film supported by a copper grid. The microscope used was a JEOL 3010UHR operated at 300 kV.

Pristine charged positive active material was studied by TEM as well. Before running TEM, this material was electrochemically activated.

### 2.8. Chemical analyses

Determination of the iron content in the positive electrode materials was made on an X-ray fluorescence spectrometer (Philips; PW2040), and the lithium concentration was determined by atomic absorption spectrometer measurements (Varian; AA 1275). The graphite content was obtained as the residue after dissolution and filtering of the material in strong hydrochloric acid. Carbonate and hydroxide ions in the electrolyte were obtained from acid–base titration.

## 3. Results and discussion

### 3.1. Ex situ XRD measurements

The XRD patterns of two of the investigated cells ([B] and [C]) follow a conventional way of structural transformation

from a discharged state to a charged state, while a third sample ([A]) does not. In Figs. 3–5, the diffraction patterns are shown of the three different float-charged cells, containing material from [A] to [C], as well as reference discharged and charged positive active material. Simple calculations considering hexagonal cells with $a = 3.13$ Å and $c = 4.61$ Å for β-Ni(OH)$_2$ (JCPDS 14-0117) and

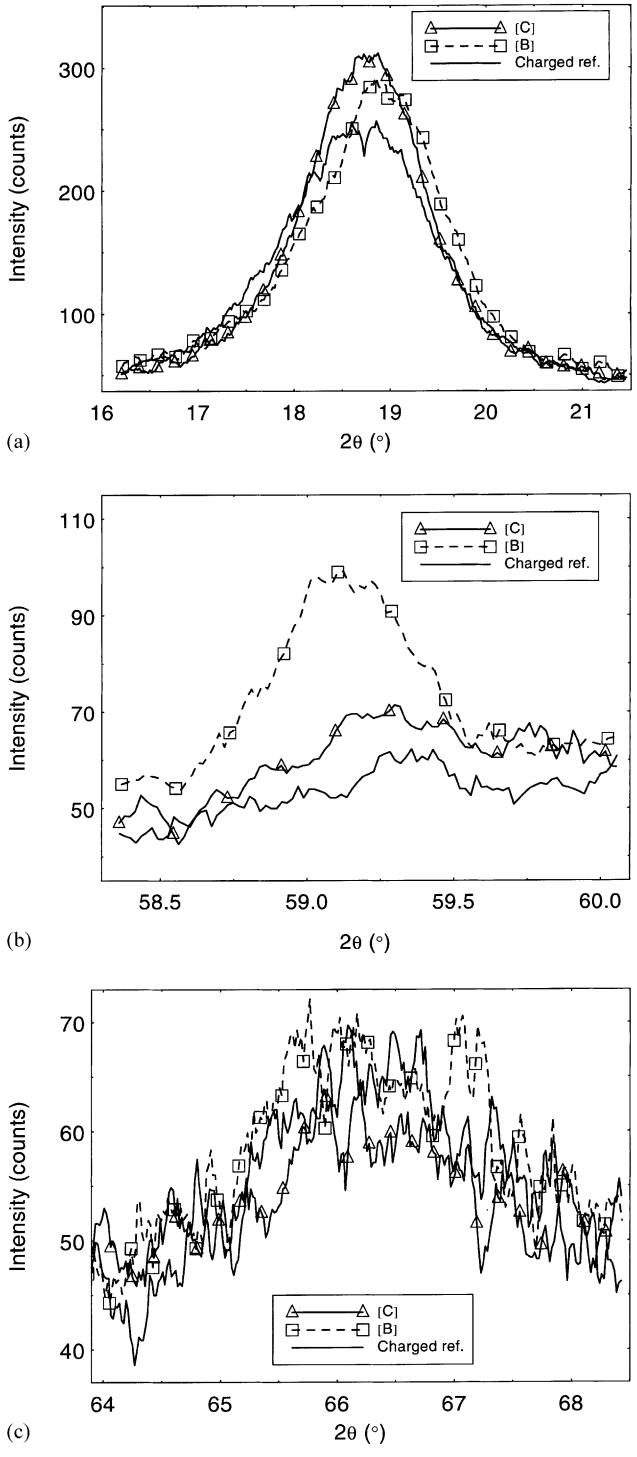


Fig. 3. XRD patterns from charged materials [B], [C] and reference: (a) (0 0 1) peak; (b) and (c) (1 1 0) peak.

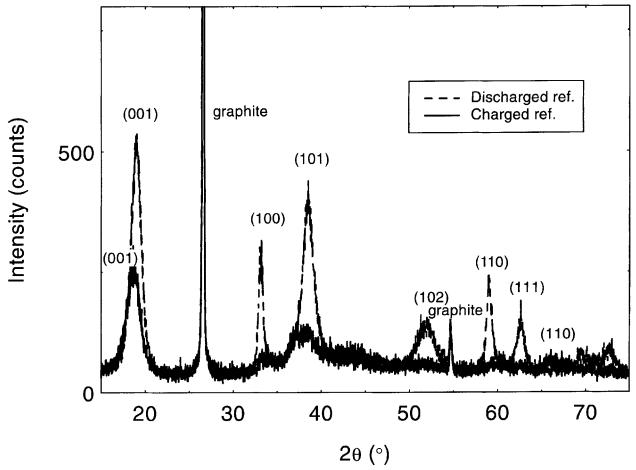


Fig. 4. Comparison of the XRD pattern obtained from charged and discharged reference active positive material.

$a = 2.81$ Å and $c = 4.84$ Å for β-NiOOH (JCPDS 06-0141) yield that the (1 1 0) peak from discharged material should appear at $2\theta = 59.2°$ and the (1 1 0) peak from charged material at $2\theta = 66.2°$. Similar calculations show that the (0 0 1) peak for the discharged state should appear at $2\theta = 19.2°$ and the charged state at $2\theta = 18.3°$. Shifts as large as these cannot be observed along (0 0 1) (Fig. 3a).

Thus, positional peak shifts in the diffraction pattern, considering the (1 1 0) and (0 0 1) peaks, are expected to occur when the active material is charged. The material [C] in Fig. 3a–c shows a large similarity with the charged reference. The (1 1 0) peak at $2\theta \approx 59°$ disappears upon charging, and the very broad peak at about $2\theta \approx 66°$ can be interpreted as the (1 1 0) peak in the charged phase. This is in accordance with a shorter *a*- and *b*-axis, and also with a largely-amorphous structure in the *ab*-plane compared to the discharged phase. A comparison of the diffraction patterns of discharged and charged reference materials (Fig. 4) shows clearly that the structure of the latter phase to a large extent is amorphous. This is indicated by the lack of well-defined Bragg peaks in the charged phase. The material [C] behaves as one would expect from current theories [9].

Fig. 5a–d show the diffraction patterns of [A], which has been charged at RT with 1.40 V for 2 years. Both the (0 0 1) and (1 1 0) peaks have positions which correspond to the β-Ni(OH)$_2$ structure, i.e. there are practically no differences from a discharged phase. Results after calculation of the crystallite sizes from (0 0 1), (1 0 0) and (1 0 1) peaks in these patterns of [A] are shown in Table 1; see also Fig. 5a. Compared to values obtained for a pristine material, it is evident that the crystallites of [A] are significantly larger after 2 years of charging at constant potential. The structure along the *c*-direction is less ordered than in the *a*- and *b*-directions. This is in complete agreement with experience of XRD analysis of positive material from aged battery cells.

The material [B] in Fig. 3a–c is shown to be partly charged, since the (1 1 0) peak at 59° in $2\theta$ still exhibits intensity. The (0 0 1) peak of [B] seems to be shifted to

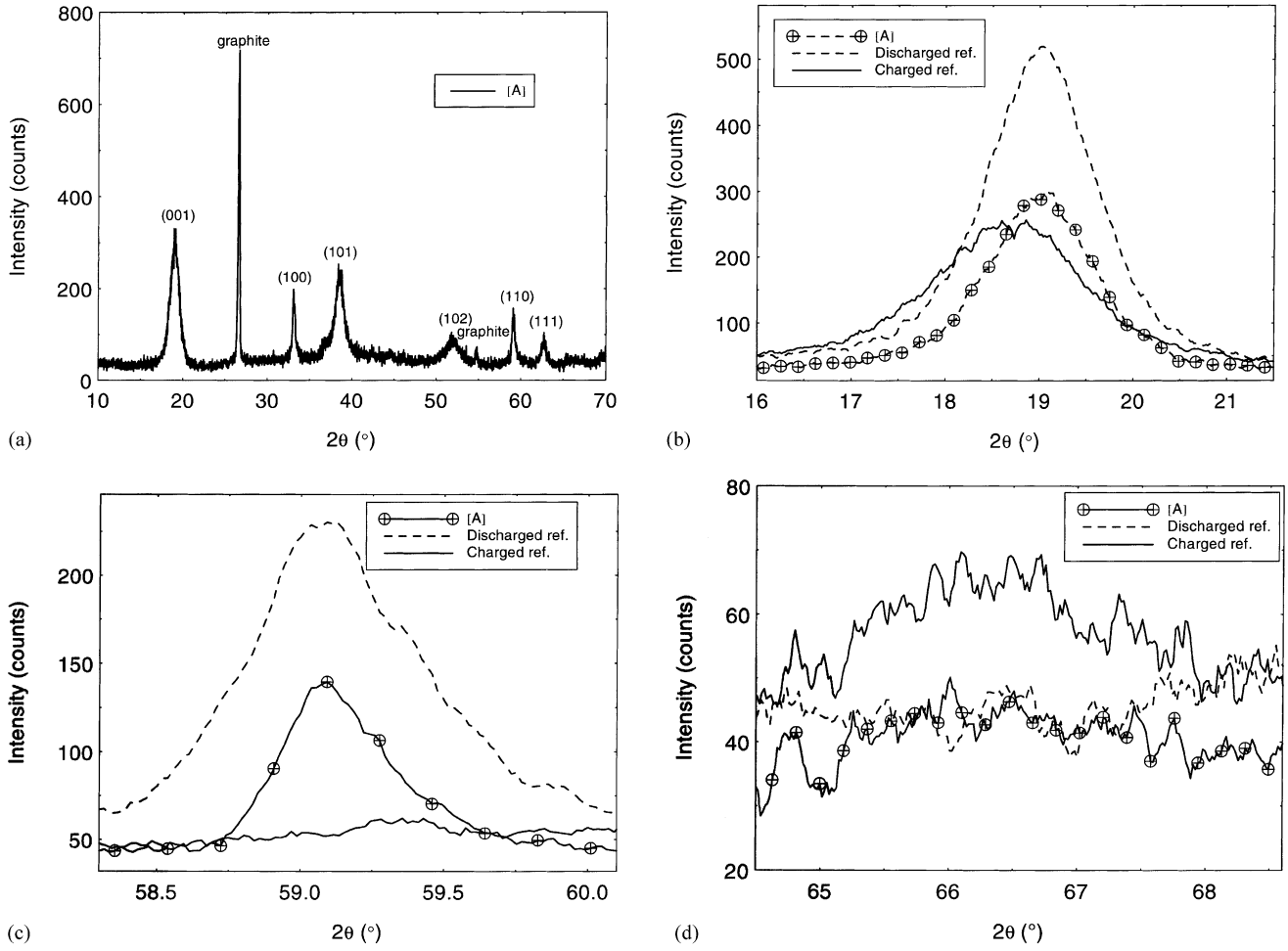


Fig. 5. XRD patterns of: (a) charged material [A]; (b) charged reference; (c) discharged reference, and (d) charged material [A]. (b) The (0 0 1) and (c–d) the (1 1 0) peaks, respectively.

higher $2\theta$ values compared to [C], which is assumed to be fully charged when compared to the charged reference cell. It should be emphasised that small shifts in peak positions are much more easily detected and preferably should be used when comparing different diffraction patterns, instead of comparing unit cell parameters derived from several peaks in a traditional cell parameter refinement. The large individual errors of the peak positions can give unreliable estimates of the cell parameters when refining cell parameters from diffraction patterns with broad and anisotropically-shaped peaks. Some peaks in the diffraction patterns of the different phases preferably should not be termed Bragg peaks in a traditional sense, but should be interpreted as a measure of how probable an interatomic distance is in the sample. Several effects such as for instance concentration gradients in the sample can give heavily-distorted peaks.

A heterogeneous charge/discharge transformation [2] is supported by these XRD results. In Fig. 3b and c, two distinct peaks are observed for material [B] at $2\theta \approx 59°$ ((1 1 0) discharged material) and $2\theta \approx 66°$ ((1 1 0) charged material) indicating the simultaneous presence of discharged and charged phases.

Table 1
Calculation of crystallite sizes (in Å) in different directions corrected for instrumental effects on peak broadening

| Sample | (0 0 1) | (1 0 0) | (1 0 1) |
|---|---|---|---|
| Discharged pristine material | 78 | 233 | 82 |
| Charged pristine material | 59 | 132 | 133 |
| Charged material [A] | 77 | 569 | 104 |

### 3.2. In situ XRD measurements

The in situ measurements on the material [A] were performed in order to avoid any effects following the drying procedure such as changed degree of hydration and the effect of oxygen in the air.

The chargeability of the cell was low; only about 30% of the positive material was charged. This low chargeability may of course increase the risk of measuring uncharged material in the electrode instead of charged material. The low value may be due to the cell construction itself, with pressed tablets leaving the innermost part of the material

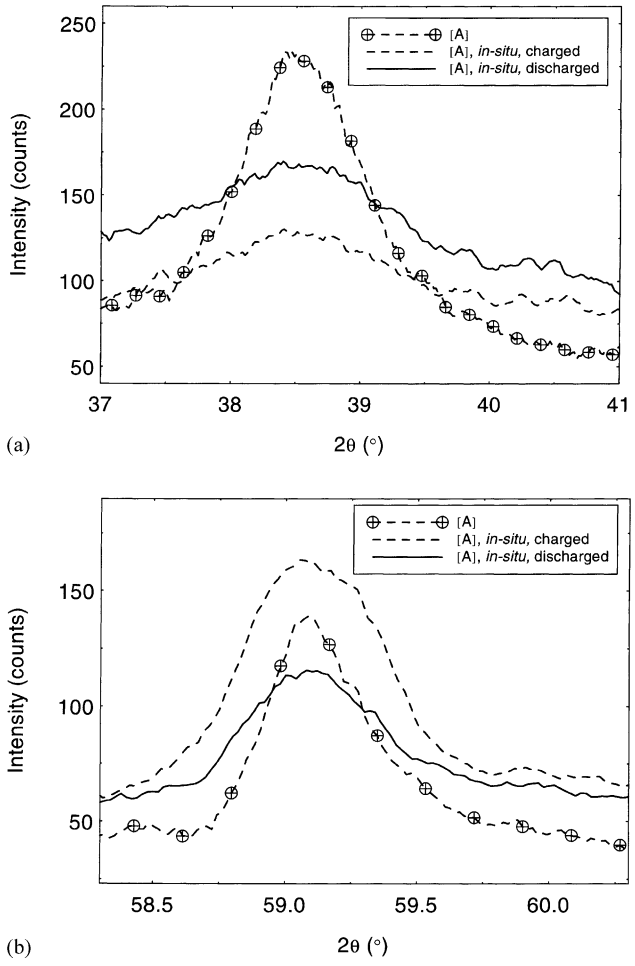


Fig. 6. In situ XRD patterns compared to ex situ patterns of material [A]: (a) the (1 0 1) diffraction peak; (b) the (1 1 0) diffraction peak.

inactive. The material at the surface contributes most to the diffraction pattern and should be most easily accessible for charging.

The results show no tendency of the diffraction pattern to shift towards the postulated β-NiOOH structure, Fig. 6a and b, which is in agreement with the results above. The (0 0 1) peak was extremely broad and heavily distorted together with an overlap from polyethylene peaks, thus it was not used in these comparisons. The (1 0 1) peak was, however, easily discernible. The (1 1 0) peak at $2\theta \approx 66^\circ$ was absent. In summary, there is a very small difference along the *ab*-direction between charged and discharged states. The conclusions regarding the *c*-direction are much more statistically inaccurate as they are based on more or less only one distorted peak (0 0 1). Furthermore, there is no differences in $2\theta$ between the resulting diffraction patterns of the active material from ex situ and in situ measurements.

### 3.3. Rietveld refinement

The XRD data of material [A] was subjected to a Rietveld refinement. β-$Ni(OH)_2$ was used as an initial model. Silicon (Si) was added to the sample and refined as a second phase in order to enable accurate estimates of the zero-point shift of the $2\theta$-scale. The cell parameter of Si was not refined but nevertheless fitted the diffraction pattern well, indicating that no serious systematic errors of the $2\theta$-scale were present. The graphite of the cell was refined as a third phase. An isotropic displacement parameter was refined for all three types of atoms in β-$Ni(OH)_2$. The positional parameters of β-$Ni(OH)_2$ were locked at the literature values [19]. The positional parameters $z$(O) and $z$(H) were thought to be well modelled by the powder neutron refinement by Greaves and Thomas [19]. The results and the parameters for the refinement are found in Table 2 and the Rietveld plot is shown in Fig. 7.

Table 2
Parameters in the Rietveld refinement

| | |
|---|---|
| $B_{iso}(Ni(OH)_2)$ (Å$^2$) | 5.4(3) |
| $B_{iso}$(Si) (Å$^2$) | 1.2 |
| Zero point error of $2\theta$ | 0.010(3) |
| $a$, $c(Ni(OH)_2)$ (Å) | 3.118(2), 4.660(4) |
| $a$(Si) (Å) | 5.4308 |
| $W(Ni(OH)_2)$ ($^{\circ 2}$) | 1.54(7) |
| $W$(Si) ($^{\circ 2}$) | 0.019(2) |
| $W$(graphite) ($^{\circ 2}$) | 0.024(1) |

The full width at half maximum (FWHM) was modelled by the usual quadratic form in $\tan(\theta)$ [20].

$$(\mathrm{FWHM})^2 = U\tan^2(\theta) + V\tan(\theta) + W$$

Due to the small number of peaks, only a separate $W$ parameter was refined for each phase. This is clearly insufficient for modelling the (*hkl*)-anisotropy of the Ni phase peaks.

Conventional Bragg $R$-values for the three phases are: $R$-$B(Ni(OH)_2) = 0.109$, $R$-$B(Si) = 0.050$ and $R$-$B$(graphite) = 0.050. The use of $R$-$B$ in favour of the more common $R$-$wP$ and $R$-$P$ is strongly recommended in order to determine how well a specific structural model fits the observed data [21].

The cell parameters of the refined charged β-$Ni(OH)_2$ phase were $a = 3.118(2)$ Å and $c = 4.660(4)$ Å. Despite a very slight deviation of the cell parameters towards the conventional charged structure ($a = 2.81$ Å and $c = 4.84$ Å JCPDS 06-0141) from the Greaves and Thomas' values for the discharged material ($a = 3.126(1)$ Å and $c = 4.593(1)$ Å), the phase is well described by the structure of the discharged β-$Ni(OH)_2$. Since the cell parameter changes are in opposite directions for the $a$ and $c$ parameters, it is not a consequence of some instrumental errors.

### 3.4. Electrochemical measurements

The results from the electrochemical investigation are shown in Table 3. For more details about the voltammetry of the active Ni material consider [14]. There are two reduction peaks observed, the first one occurred at a potential of 200 mV versus Ag/AgCl reference electrode corresponding

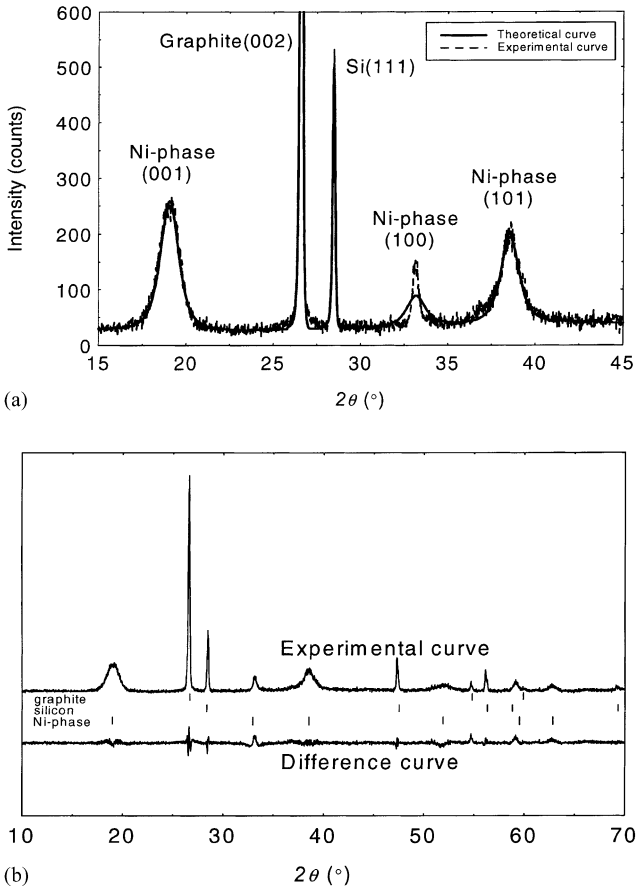


Fig. 7. (a) Experimentally-determined XRD pattern of the charged material [A] compared to a theoretical pattern calculated using the results from the Rietveld refinement; note the narrow (1 0 0) peak. (b) The results from the Rietveld refinement, a difference curve (bottom curve) together with the observed experimental diffraction pattern (upper curve). In the figure, the theoretical peak positions of graphite, silicon and β-$Ni(OH)_2$ are shown.

to the reduction of β-NiOOH to β-$Ni(OH)_2$. The second peak occurred at a potential of −440 mV corresponding to the reduction of β-$Ni(OH)_2$ to nickel metal. The amount of charge, the area of the peaks, was calculated for the two reduction peaks. The area of the second peak was about twice as large as the area of the first one. The reason for this is that the electron transfer for the second reaction is a two-electron transfer $Ni(II) \rightarrow Ni(0)$, while that of the first one is a one-electron transfer $Ni(III) \rightarrow Ni(II)$. A simple calculation shows that the sample initially contained about 80% of the charged material. This concludes that the material was almost fully charged, since a charged battery cell to some extent also contains minor amounts of the discharged phase. The CPEE method reduces all materials at the electrode surface, i.e. even material that is not utilised in the battery. The same conclusion could be made from the chronopotentiometry experiments.

Table 3
The potential and amount of charge for the reduction steps in the electrochemical investigation of material [A]

| Reaction | No. of $e^-$ (in electron transfer) | Potential (mV) vs. Ag/AgCl | Charge (mQ) |
|---|---|---|---|
| β-NiOOH → β-$Ni(OH)_2$ | 1 | 200 | 480 |
| β-$Ni(OH)_2$ → Ni | 2 | −440 | 1220 |

### 3.5. TEM measurements

TEM was performed on discharged [A] and pristine charged positive material. The material was washed in water and dried at 70°C overnight before insertion in the microscope. It should be emphasised that this treatment, the sample preparation (ethanol is a reducing agent) as well as the high vacuum, the elevated temperature and the beam itself inside the microscope are parameters that may affect the specimen. During the time scale of the experiment, we could not observe any radiation damage of the sample.

In Fig. 8, a low magnification picture is presented showing the shape of the β-$Ni(OH)_2$ particles. The prolonged crystallite is rod shaped and growing along the *c*-axis. In Fig. 9a, a perfectly aligned selected aperture electron diffraction (SAED) pattern along the [1 0 0] zone axis is shown, indicating a well ordered and crystalline material. A careful study of the reciprocal space in these crystals indicates that the lattice parameters and symmetry are significantly different compared to the data reported (JCPDS 14-0117). The indexing of the [1 0 0] zone axis (Fig. 9a) resulted in a *c*-axis equal to 5.0(1) Å (five randomly-chosen crystals were used for the calculation), which should be compared with the tabulated value $c = 4.605$ Å (JCPDS 14-0117). The length of the *b*-axis did not deviate from the tabulated value obtained by powder diffraction. It should be mentioned that although the precision of TEM is below powder X-ray or neutron diffraction, the differences observed are significant.

Tilt experiments around the principal directions in the [1 0 0] zone axis were performed in order to avoid double diffraction and to enable the study of possible translational symmetry elements [22]. Forbidden or systematically absent reflections in X-ray and neutron diffraction patterns, due to translational symmetry elements, can exhibit intensity in SAED pattern as a consequence of double diffraction. That is, a diffracted beam can act as a new primary beam and be re-diffracted when travelling through the crystal. This can occur only when the crystal is well aligned with respect to a crystallographic direction. Tilting the crystal out of the crystallographic direction eliminates double diffraction and makes it possible to study translational symmetry elements. In Fig. 9a, the perfectly-aligned SAED pattern along [1 0 0] is shown. In Fig. 9b and c, the results of the tilting experiments are shown. Note that the reflections along [0 0 1] with $l = 2n + 1$ are missing in Fig. 9b. In Fig. 9c, all reflections are present. These results indicate that the discharged material [A] should have a translational symmetry element along the [0 0 1] direction in contrast to what is reported for β-$Ni(OH)_2$, *P31m* (1 6 2) [9,19].

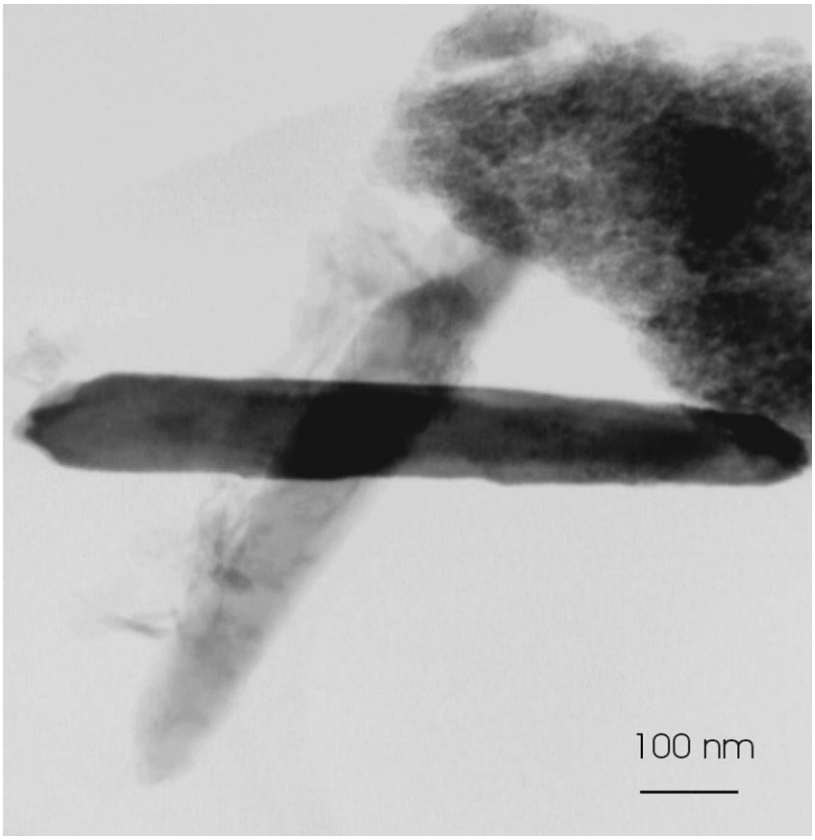


Fig. 8. Low magnification TEM image of a β-$Ni(OH)_2$ crystal [A] (discharged), horizontal in the figure, showing the rod-like appearance along the [0 0 1] axis.

Convergent beam electron diffraction (CBED) measurements are in progress in order to determine the correct space group, and will be reported elsewhere.

TEM investigations on pristine charged material show no crystalline order at all.

### 3.6. Chemical analyses

The relatively high Fe content in the positive active materials [B] and [C] (see Table 4) may affect the performance of the cell and lower the overvoltage of oxygen evolution, and therefore, somewhat decrease the positive electrode capacity to a final voltage of 1.5 V versus Zn/ZnO. However, in the present case the main reason to the decreased chargeability was found to be carbonation of the graphite in the positive material; Ahlberg et al. [14]. The iron and carbonation effects mentioned above ought to make the materials [B] and [C] more similar with respect to the structure of the discharged phase. This is not observed in our diffraction patterns. From the interpretation of the diffraction patterns, the [B] and [C] materials are similar to the conventional charged β-NiOOH phase despite the low chargebility of [B] and [C]. Material [A] is on the contrary similar to the discharged phase even though this material exhibits the best capacity, the lowest degree of carbonation and the lowest Fe content (see Table 4). By considering the nominal capacity of the [A] positive electrode and comparing the value with the experimentally determined electrode

Table 4
Chemical analyses and capacity measurements of the positive active materials

| Material | Test background[a] | Nominal capacity (Ah) | Experimentally-determined nominal capacity[b] (%) | Degree of carbonation[c] (%) | Fe content (wt.%) |
|---|---|---|---|---|---|
| A | 1.42 V/RT/2 years | 145 | >95 | 13 | 0.05 |
| B | 1.40 V/40°C/3 years | 114 | 59 | 57 | 0.49 |
| C | 1.42 V/40°C/3 years | 131 | 37 | 46 | 0.40 |

[a] Float-charged at a certain potential/temperature/time in operation.
[b] Capacity at potential 1.50 V vs. Zn/ZnO reference electrode.
[c] Calculated as the concentration ratio of $K_2CO_3$ and $\sum(K_2CO_3, KOH, LiOH)$.

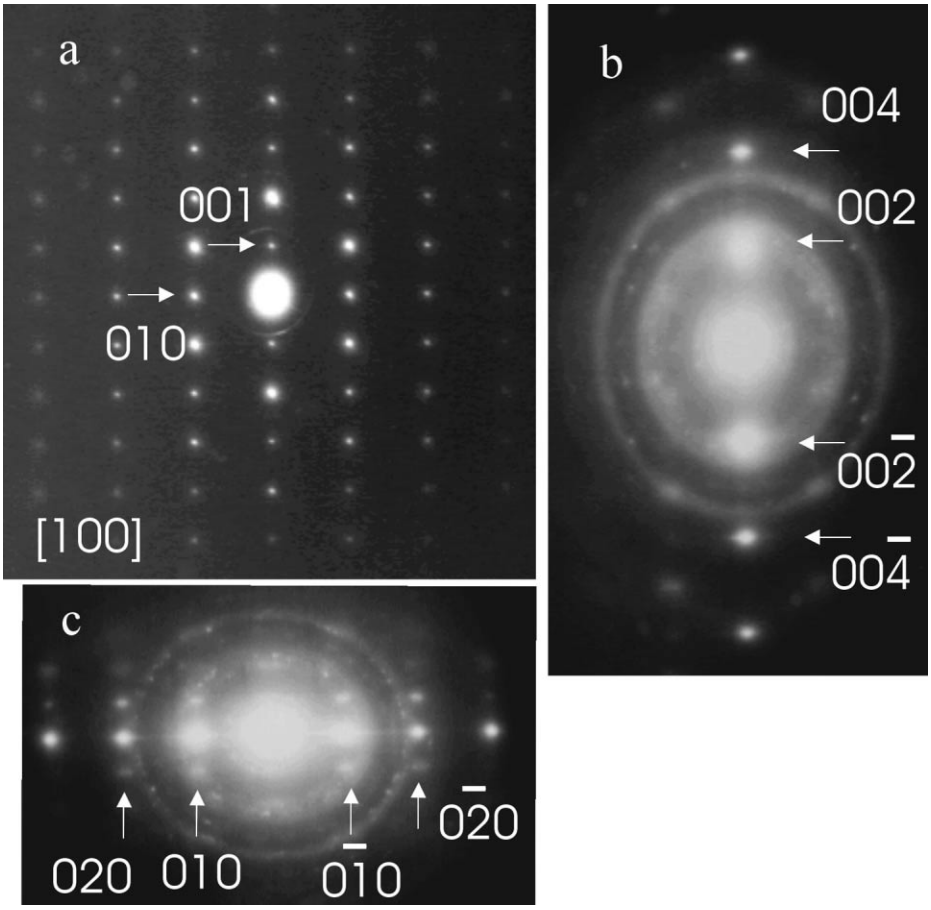


Fig. 9. (a) SAED pattern along the [1 0 0] direction, and (b) and (c) correspond to the same pattern, but slightly tilted. In (b) the [0 0 1] row and in (c) the [0 1 0] row is kept fixed. Notice how the reflections with $l = 2n + 1$ are missing in (b) and that no reflections are missing in (c).

capacity after 2 years of float charging, more than ~95% of the available nickel is still electrochemically active. From these calculations, one can assume that the amount of discharged material after charging is rather small, and should not significantly contribute to the X-ray diffraction pattern.

The Li content in the positive active material should not cause any performance problem as the Li/Ni ratio is very low, less than or equal to 0.007. Briggs [23] claims that a ratio above 0.08 should be detectable by XRD as lithium nickelate, $LiNiO_2$. We did not observe any contributions from $LiNiO_2$.

## 4. Conclusions

In this study, three different aged electrodes from pocket plate single cells have been investigated. The results illustrate the difficulties when using diffraction methods and when characterising the positive active Ni material, especially the charged phase. The structures of the Ni material may depend on several parameters: temperature, working potential, time in use in working conditions, and the content of the electrolyte, etc. In two cases out of three, the charged phases exhibit a diffraction pattern consisting of three broad peaks. The peak positions can be used to calculate a hexagonal unit cell. This is mathematically possible but not reliable. To calculate a unique model from these amorphous materials is then unreasonable and impossible.

This study also shows the existence of a charged nickel hydroxide phase with a diffraction pattern similar to the diffraction pattern of the conventional β-$Ni(OH)_2$. The charged state was confirmed by electrochemical measurements. Several different structure models could be possible, for example the β-$Ni(OH)_2$ structure used in this study for the Rietveld refinements of a structure model of the charged material [A]. Still another structure model of the charged phase β-NiOOH would be small domains of $NiO_2$ and β-$Ni(OH)_2$ giving the overall stoichiometry of β-NiOOH. It must be emphasised that the structure of β-NiOOH is essentially unknown. The domains could be randomly oriented and causing an average structure giving a diffraction pattern similar to those observed for [B] and [C]. Consequently, it is unrealistic to talk about a unique structure model of the charged phase.

Broad diffraction peaks should at some point (of broadness) no longer be interpreted as Bragg peaks, but more as a general probability of finding a repetition distance in the structure. One can interpret these broad peaks in a traditional sense as for a well-crystalline compound, but for the structural model to be complete for as amorphous samples as the charged Ni electrode material one should also have some idea about the disorder evidently present. One way to accomplish this goal would be to investigate the total scattering from an electrode sample using reverse Monte-Carlo modelling (RMC).

The most reliable method for investigation of local structure from ordered as well as disordered materials is TEM investigations, if one can handle the additional difficulties (sample preparation, radiation damage, the sample containment, etc.) connected with TEM. The X-ray powder diffraction method works very well for crystalline ordered materials where the information from the disordered part of the compound is hidden in the background level.

The results from the TEM investigations of well-crystalline samples of the discharged material [A] show structural dissimilarities to the normal β-$Ni(OH)_2$ structure. The charged phase of pristine positive material was completely amorphous in the TEM. With the observation that the sample is amorphous even at the length scale attainable in the TEM, it is most difficult to understand the correctness of assigning crystal structure models to the charged phase from powder diffraction data. This phase must be studied with methods either sensitive to the local structure (TEM) or with methods taking into account even the information in the background (liquid, paracrystalline modelling with the RMC). The deviations of the structure of the discharged material [A], studied in the TEM, compared to the normal β-$Ni(OH)_2$ structure are small. Probably, a good fit to the X-ray diffraction pattern of the normal β-$Ni(OH)_2$ can be obtained with a slightly different structure model. Further investigations are in progress to better determine space group and structural parameters for the discharged material [A], and also to look for common structural features from different indistinguishable models of the amorphous diffraction pattern of the charged phase.

## Acknowledgements

We are grateful to people at Saft AB in Oskarshamn for their contribution throughout the course of this study.

## References

[1] S.U. Falk, A.J. Salkind, Alkaline Storage Batteries, Wiley, New York, 1969.
[2] C. Léger, C. Tessier, M. Ménétrier, C. Denage, C.J. Delmas, J. Electrochem. Soc. 146 (1999) 924.
[3] E.A. Charles, The effects of cobalt hydroxide addition on the nickel hydroxide electrode, Ph.D. Thesis, University of Newcastle upon Tyne, 1989.
[4] G.W.D. Briggs, W.F.K. Wynne-Jones, Electrochim. Acta 7 (1962) 241.
[5] R.S. McEwen, J. Phys. Chem. 75 (1971) 1782.
[6] R. Barnard, G.T. Crickmore, J.A. Lee, F.L. Tye, J. Appl. Electrochem. 10 (1980) 61.
[7] W. Feitknecht, H.R. Christen, H. Studer, Z. Anorg. Chem. 238 (1956) 88.
[8] H. Bode, K. Dehmelt, J. Witte, Electrochim. Acta 11 (1966) 1079.
[9] International Centre for Diffraction Data (ICDD), Newton Square, PA, USA.
[10] P. Oliva, J. Leonardi, J.F. Laurent, C.J. Delmas, J.J. Braconnier, M. Figlarz, F. Fievet, A. de Guibert, J. Power Sources 8 (1982) 229.
[11] A.N. Mansour, C.A. Melendres, M. Pankuc, R.A. Brizzolara, J. Electrochem. Soc. 141 (1994) L69.
[12] A.M. Malsbury, C. Greaves, J. Solid State Chem. 71 (1987) 418.
[13] N. Sac-Epée, M.R. Palacín, A. Delahaye-Vidal, Y. Chabre, J.-M. Tarascon, J. Electrochem. Soc. 145 (1998) 1434.
[14] E. Ahlberg, U. Palmqvist, N. Simic, R. Sjövall, J. Power Sources 85 (2000) 245.
[15] P. Scherrer, Gött. Nachr. 2 (1918) 98.
[16] A.H. Nahlé, F.C. Walsh, C. Brennan, K.J. Roberts, J. Appl. Cryst. 32 (1999) 369.
[17] N. Simic, E. Ahlberg, J. Electroanal. Chem. 451 (1998) 237.
[18] N. Simic, R. Sjövall, U. Palmqvist, E. Ahlberg, J. Power Sources 94 (2000) 1–8.
[19] C. Greaves, M.A. Thomas, Acta Cryst. B 42 (1986) 51.
[20] G. Caglioti, A. Paoletti, F.P. Ricci, Nucl. Instrum. 3 (1958) 223.
[21] L. Eriksson, D. Louër, P.-E. Werner, J. Solid State Chem. 81 (1989) 9.
[22] D.B. Williams, C.B. Carter, Transmission Electron Microscopy, Plenum Press, New York, 1986.
[23] G.W.D. Briggs, Chem. Soc. Spec. Period. Rep., Electrochemistry 4 (1974) 33.